Multifunctional composites using reinforced laminae with carbon-nanotube forests

VINOD P. VEEDU[1]*, ANYUAN CAO[1], XUESONG LI[2], KOUGEN MA[1], CATERINA SOLDANO[2], SWASTIK KAR[2], PULICKEL M. AJAYAN[2]* AND MEHRDAD N. GHASEMI-NEJHAD[1]*

[1]Hawaii Nanotechnology Laboratory, Department of Mechanical Engineering, University of Hawaii at Manoa, 2540 Dole Street, Holmes Hall 302, Honolulu, Hawaii 96822, USA
[2]Department of Materials Science & Engineering, Rensselaer Polytechnic Institute, Troy, New York 12180, USA
*e-mail: vinodpv@hawaii.edu; ajayan@rpi.edu; nejhad@wiliki.eng.hawaii.edu

Published online: 7 May 2006; doi:10.1038/nmat1650

Traditional fibre-reinforced composite materials with excellent in-plane properties fare poorly when out-of-plane through-thickness properties are important[1]. Composite architectures with fibres designed orthogonal to the two-dimensional (2D) layout in traditional composites could alleviate this weakness in the transverse direction, but all of the efforts[1,2] so far have only produced limited success. Here, we unveil an approach to the 3D composite challenge, without altering the 2D stack design, on the basis of the concept of interlaminar carbon-nanotube[3,4] forests that would provide enhanced multifunctional properties along the thickness direction. The carbon-nanotube forests allow the fastening of adjacent plies in the 3D composite. We grow multiwalled carbon nanotubes on the surface of micro-fibre fabric cloth layouts, normal to the fibre lengths, resulting in a 3D effect between plies under loading. These nanotube-coated fabric cloths serve as building blocks for the multilayered 3D composites, with the nanotube forests providing much-needed interlaminar strength and toughness under various loading conditions. For the fabricated 3D composites with nanotube forests, we demonstrate remarkable improvements in the interlaminar fracture toughness, hardness, delamination resistance, in-plane mechanical properties, damping, thermoelastic behaviour, and thermal and electrical conductivities making these structures truly multifunctional.

For many decades, advanced fibre-reinforced polymer and ceramic-matrix composites have been used as viable primary load-bearing structures. Although the in-plane loading and stresses have been handled by various configurations of fibre architectures, such as 1D (that is, unidirectional tapes) and 2D (that is, woven fabrics), the intralaminar and interlaminar stresses have remained major issues, resulting in relatively weak interlaminar fracture toughness. This weakness often leads to interlaminar failures, such as delamination, in composites under various loading conditions. To solve these significant challenges, researchers have developed 3D braided fibres as well as through-thickness stitching[1,2]. These approaches have problems, such as low in-plane strengths for the 3D braided fibres[2] and shorter tensile fatigue life[5] and lower compression strengths for the stitched fibre laminates[6].

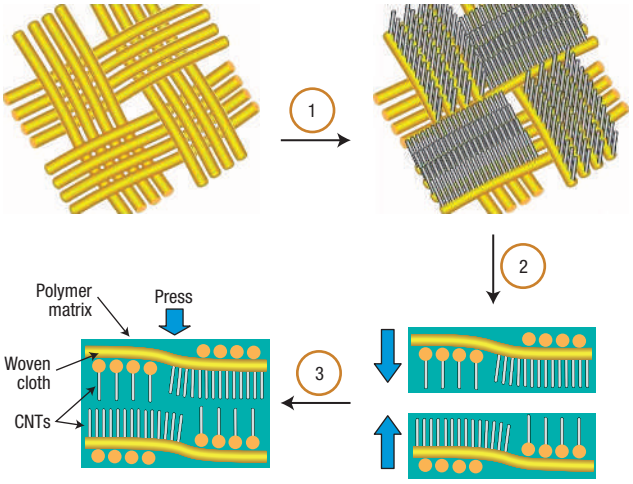

Figure 1 Schematic diagram of the steps involved in the hierarchical nanomanufacturing of a 3D composite. (1) Aligned nanotubes grown on the fibre cloth. (2) Stacking of matrix-infiltrated CNT-grown fibre cloth. (3) 3D nanocomposite plate fabrication by hand lay-up.

Different studies using carbon-nanotube reinforcements in polymer composites[7–11] have reported small improvements in the bulk mechanical properties compared with traditional fibre-reinforced composites. However, the real use of nanotubes in composites for structural applications has been disappointing, despite huge promise, due to issues such as dispersion, alignment, and interfacial strength[8,11]. Here, we demonstrate an unexplored yet big opportunity for nanotubes in composites, to influence and increase the 3D composite interlaminar properties, using unique reinforced laminae with carbon-nanotube forests grown on fibres present in adjacent plies. To optimize this interfacial effect, we grow well-aligned multiwalled carbon nanotubes (CNTs) perpendicular to 2D woven fabrics of SiC to produce 3D fabrics. For the growth of

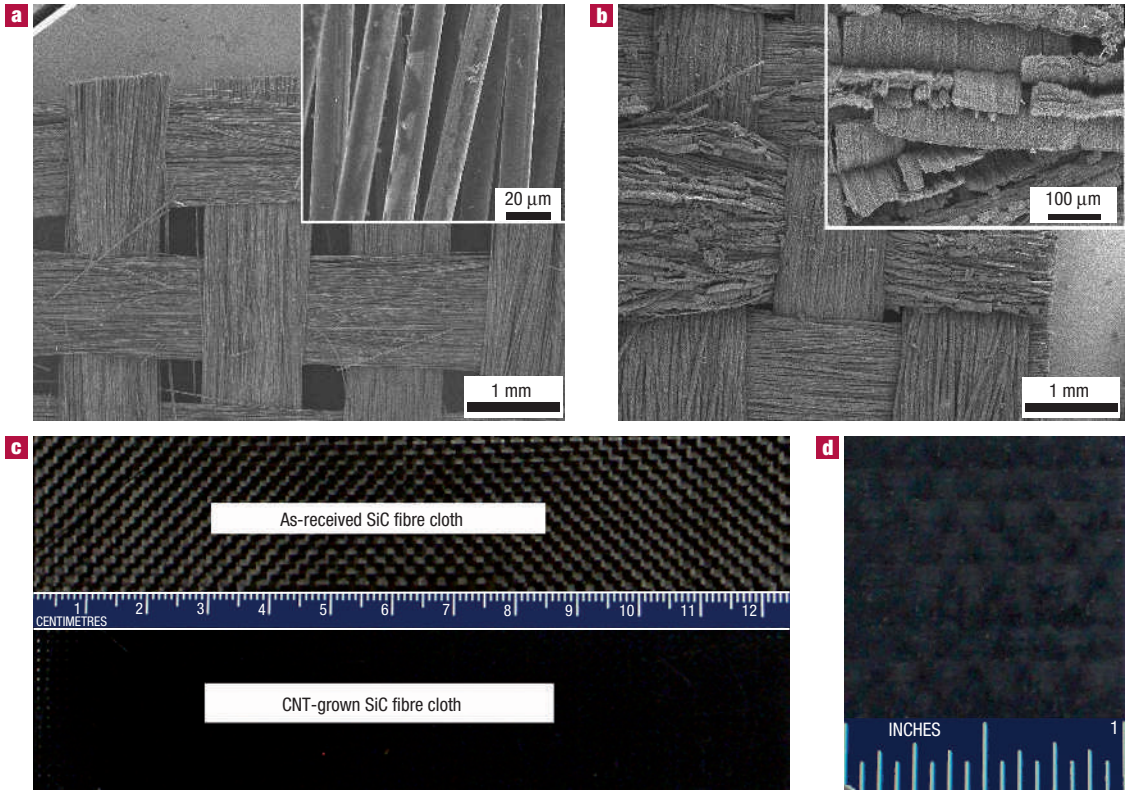

Figure 2 The growth of CNTs on the SiC woven cloth. a, Plain-weave SiC fabric cloth. Inset: individual fibres of the woven cloth. **b**, The cloth with CNTs grown perpendicularly on its surface. Inset: close-up. **c**, Photographs showing an as-received SiC fibre cloth and CNT-grown SiC fibre cloth. **d**, Photograph of a 1 × 1 inch 3D composite laminate from stacking of two laminae shown in **c**.

CNTs on SiC woven cloth, we used the chemical-vapour-deposition (CVD) process[12] (see Supplementary Information, Fig. S1). These fabrics are then infiltrated by a high-temperature epoxy matrix, and are subsequently stacked[13] to form multilayered 3D composites (see Fig. 1 and Supplementary Information).

Figure 2a shows a scanning electron micrograph of the top of a piece of SiC fibre cloth consisting of 16-μm fibres (see inset) woven into a 2D plain-weave fabric[13]. The SiC fibre cloth after growing CNTs on its surface, by the CVD process, is shown in Fig. 2b (a close-up view is shown in the inset of Fig. 2b). CNTs are grown uniformly on all of the exposed fibres on the surface of the fibre cloth[14]. The nanotubes grown on the fibres were about 60-μm long (see Supplementary Information, Fig. S2). The use of various fibre cloth weave patterns will affect the alignment of the CNTs in the laminate thickness direction, where the degree of CNT alignment will increase as the number of the weave-harness increases, which in turn will affect the through-thickness properties of the composites. We have successfully grown CNTs uniformly on SiC fibre cloths of up to 120 mm × 40 mm (see Fig. 2c) and this is very scalable for larger dimensions. The nanotube-grown fabrics were infiltrated with a high-temperature epoxy, then stacked to yield a 'sandwich' structure, and the laminated structure was cured in an autoclave at a maximum of 150 °C for 1 h (see the Supplementary Information). Generally, the proposed fabric reinforcement can be infiltrated with polymers or preceramic polymers[13,15,16] with appropriate viscosities to produce polymer-matrix or ceramic-matrix composites, respectively. An optical photograph of the fabricated 3D composite sandwich (1 × 1 inch) is shown in Fig. 2d. The weight fractions of the matrix, SiC and CNTs in the fabricated 3D composites are 35%, 63% and 2%, respectively.

Several experiments were carried out to demonstrate the transverse mechanical properties improvement, and the effect of the CNT forests bridging the plies. To demonstrate the fibre-bridging effect due to the nanotube forests, an interlaminar fracture toughness test was carried out in which the composite specimen was loaded so that the laminates were pulled apart yielding the opening mode (that is, Mode I; ref. 17) fracture toughness measure, G_{IC} (ref. 17). We used a double-cantilever beam (DCB) test based on the American Society for Testing and Materials (ASTM) standard D5528 (see the Methods section). Two different specimens, that is, a base composite (stacked laminates with no nanotubes) and the 3D composite, were tested for comparison. To measure the interlaminar sliding shear fracture toughness of the laminated composites, an end notched flexure (ENF)[17] test was carried out (see the Methods section). To apply shear load, the specimen was loaded in three-point flexure. The specimen dimensions used were the same as those used in the DCB test (including the pre-crack). To characterize the local behaviour of the base composite and the 3D reinforced composite, we measured (see the Methods section) the hardness and indentation modulus using a nanoindenter dynamic-contact module.

Figure 3a shows the load versus deflection from the DCB test. For the same applied load, the deflection is far less in the 3D composite compared with its base counterpart, indicating much higher interlaminar fracture toughness for the 3D composite. As only the first value of G_{IC} represents generic interlaminar fracture toughness[18,19] in this work, we report fracture

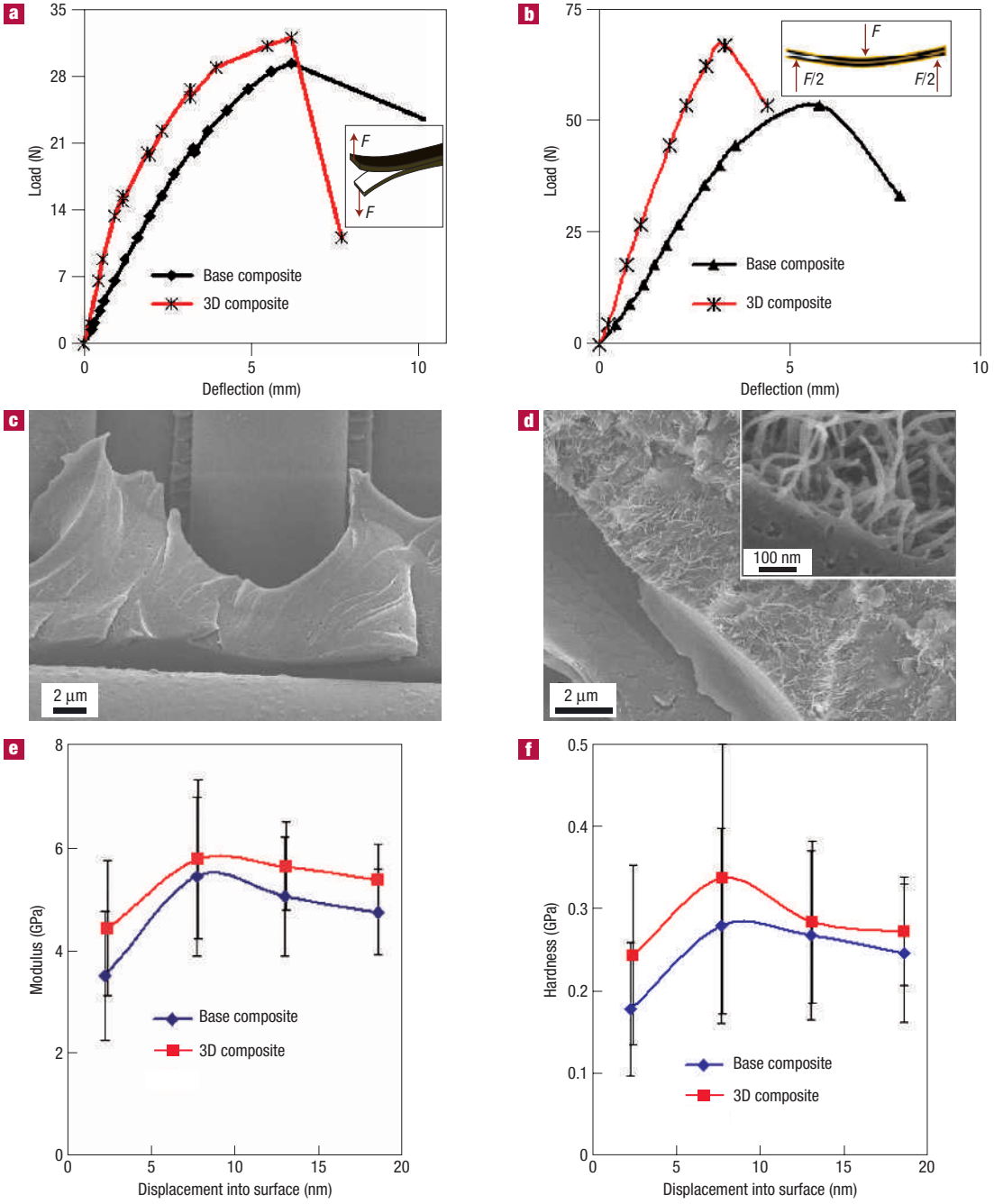

Figure 3 Fracture-toughness experimental results and fracture-surface images of base composite and 3D composite. a, Load versus deflection from the DCB test. **b**, Load versus deflection from the ENF test. **c**, Fracture-surface image of the base composite from the DCB test. **d**, Fracture-surface image of the 3D composite from the DCB test. Inset: close-up view showing the nanotubes pulled out of the matrix. **e**, Indentation modulus results from the nanoindentation tests of the 3D composite and the base composite for an average loading range of 0.000115–0.0025 mN (that is, an indentation depth range of 2.5–18.5 nm). **f**, Plot showing the hardness results from the indentation tests of the 3D composite and the base composite for an average loading range of 0.000115–0.0025 mN (indentation depth range of 2.5–18.5 nm). The mean value of indentation modulus and hardness versus displacement into surface for the ten indentation experiments on a particular sample were determined over a discrete displacement window of approximately 5 nm. In **e** and **f**, the *Y*-error bars represent the standard deviation about the mean value for the selected window.

toughness (G_{IC}) as the initial value with crack propagation. From the fracture-toughness values calculated, the 3D composite shows a G_{IC} of 4.26 kJ m^{-2}, that is, 348% improvement compared with the base composite with a G_{IC} of 0.95 kJ m^{-2} (see Table 1). The interlaminar shear sliding fracture toughness, G_{IIC}, measured from the ENF test[17] was calculated at the onset of nonlinearity (see Fig. 3b). The G_{IIC} measure of the 3D composite (140 J m^{-2}) is improved by about 54% compared with the base specimen (91 J m^{-2}) (see Table 1).

An investigation of the scanning electron micrographs of the fracture surface of the base composite (Fig. 3c) and the 3D composite (Fig. 3d) reveals that the superior fracture performance

Table 1 Comparison of the results from the fracture-toughness experiments, flexural test, structural dynamic properties, average CTE, as well as through-thickness thermal and electrical conductivities of the 3D composite specimens.

Material property type		Base composite	3D composite
Fracture-toughness test results	G_{IC} (kJ m^{-2})	0.95	4.26
	Enhancement in G_{IC}		348%
	G_{IIC} (J m^{-2})	91	140
	Enhancement in G_{IIC}		54%
Flexure test results	Flexural modulus (GPa)	$23.1 \pm 0.3 = 100\%$	$24.3 \pm 0.2 = 105\%$
	Flexural strength (MPa)	$62.1 \pm 2.1 = 100\%$	$150.1 \pm 1.4 = 240\%$
	Flexural toughness (N mm)	$5.8 = 100\%$	$30.4 = 524\%$
Structural dynamic properties	f_m (Hz)	753.8	598.2
	ζ	0.0095	0.0731
	f_n (Hz)	753.9	601.4
	$f_n\zeta$	7.162	43.963
	Enhancement in damping		514%
Average CTE over 0–150 °C (p.p.m. °C^{-1})		$123.9 \pm 0.4 = 100\%$	$47.3 \pm 0.3 = 38\%$
Through-thickness thermal conductivity at 125 °C (W m^{-1} K^{-1})		$0.33 = 100\%$	$0.5 = 151\%$
Through-thickness electrical conductivity (S cm^{-1})		0.075×10^{-6}	0.408

of the 3D composite results from a mechanical interlocking between the fibres and the matrix by means of the nanotubes. The interlocking effect between the adjacent plies due to the CNT forests (see inset in Fig. 3d) makes it difficult to open the plies, leading to the high interlaminar fracture toughness, G_{IC}, of the 3D composite. The effect of the CNT forests on G_{IIC} (that is, 54% enhancement) is not as pronounced as it is on G_{IC} (that is, 348% enhancement), which may be attributed to the shearing effect of the matrix at the base of the CNTs for G_{IIC} (see inset in Fig. 3b) rather than the strong 'pulling-apart' of the CNT forests for G_{IC} (see inset in Fig. 3a).

The spatial heterogeneity in the composite specimens is reflected in the fluctuation of the indentation results with displacement-into-the-surface of the specimens (see Fig. 3e,f). The consistent enhancement in the indentation modulus (see Fig. 3e) as well as the hardness (see Fig. 3f) of the 3D composite compared with the base composite for all indentation depths is clear (also see the Supplementary Information). At the lower indentation depth, that is, at an approximate indentation depth of 2.5 nm, the percentage improvements in the indentation modulus and hardness of the 3D composite compared with those for the base sample were 30% and 37%, respectively (see Fig. 3e,f). The possibility of partial misalignment of the CNTs during the fabrication of the 3D composite suggests that these properties can be improved even further on optimization.

The composite specimens were tested under a three-point flexural loading[17], based on the standard ASTM D790-00, to measure the in-plane mechanical performance. The measured in-plane strength, modulus and toughness of the 3D composite show 140%, 5% and 424% enhancements compared with the base composite (see Table 1 and Supplementary Information, Fig. S3), indicating that the enhancement of the through-thickness mechanical properties does not compromise the in-plane properties.

In addition to the large-scale improvements in mechanical properties, the 3D composite also shows superior multifunctional performances such as damping, coefficient of thermal expansion (CTE), and thermal and electrical conductivities. Damping is the dissipation of vibrational energy under cyclic loading. Inducing damping in a structure would essentially improve the fatigue life of the system. CNTs have been strong candidates for structural-damping applications[20–22]. Here, we measure (see Fig. 4a and Supplementary Information) and compare the natural frequencies as well as the damping ratios of the 3D composite with those of its 2D counterpart using a cantilevered-specimen (see inset Fig. 4a) experiment. The data in Table 1 compare the results of structural dynamic properties of the 3D composite as well as the base composite, where f_n and ζ are the natural frequency and damping ratio, respectively (see Supplementary Information for details). It is seen that the nanotube-fastened 3D composite has improved ζ by 669% compared with the 2D composite (see Table 1). In addition, the damping characteristics, $f_n\zeta$, enhancement is more than five times (that is, 514%) for the 3D composite compared with the base counterpart. This result is very encouraging for the use of 3D nanotube composites in many structural areas where structural damping is highly desired.

In traditional fibre-reinforced composites, thermal expansion, in all but the transverse direction, of the laminates can be controlled by varying the volume fraction and orientation of the fibres. However, large thermal expansion in the transverse direction is undesirable but difficult to control. In our 3D composite, we expect to have better control of the thermal expansion in the transverse direction, and thereby better dimensional stability due to the presence of CNT forests in the perpendicular direction of the fibres. CNTs themselves have a negative coefficient of thermal expansion[9,23]. To characterize the through-thickness thermoelastic dimensional stability of the composite specimens, we determined the CTE, that is, the fractional change in length per unit rise in temperature, of the two composite systems (3D composite and the base specimen). Measurements were made with a Michelson laser interferometer measurement system based on ASTM Standard E289–95 carried out under vacuum (see the Methods section). The through-thickness microstrain versus temperature is plotted in Fig. 4b. Each microstrain versus temperature plot shows data for several heating/cooling cycles. The average slope over a finite temperature range, in our case 0–150 °C, can be obtained to give an average CTE for the specimen (see Table 1). The test results suggest that the presence of CNTs in the thickness direction of the 3D composites reduced the CTE from 123.9 ± 0.4 to 47.3 ± 0.3 p.p.m. °C^{-1} (that is, a reduction to 38% of the original value), which is attributed to the effect of interfacial CNTs in resisting expansion of the plies through fastening interactions.

Through-thickness thermal conductivities of the base composite and the 3D composite were also measured for comparison. The thermal conductivity of the composite specimens was characterized using a UNITHERM Model 2022 following the ASTM standard E1530. Figure 4c plots the thermal conductivity

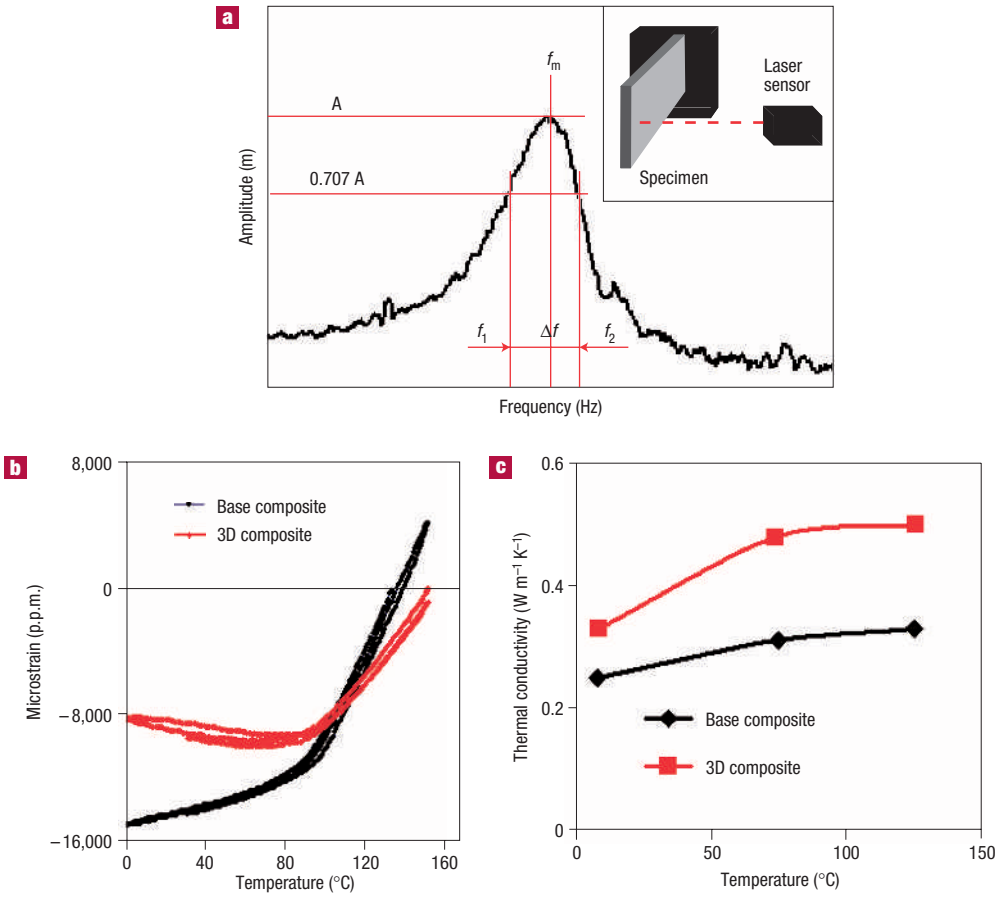

Figure 4 Demonstration of multifunctionalities exhibited by the 3D composite. a, Structural dynamic analysis of the composite specimens: typical amplitude versus frequency plot from the experiment. Inset: experimental setup for measuring the natural frequency and damping ratio of composite specimens. The dimensions of the specimens tested were 21.65 mm × 1.25 mm × 25.4 mm. **b**, Through-thickness thermal strain versus temperature graphs for the 3D and base composite specimens (the results have an uncertainty of ±1.5% for 95% confidence level). **c**, Through-thickness thermal conductivity versus temperature results for the 3D and base composite specimens. (The results have an uncertainty of ±3% for 95% confidence level.)

at different desired temperatures (8, 75 and 125 °C). The thermal conductivity of the 3D composites shows consistent improvements compared with the base composite at all temperatures. Here, it is noteworthy that the high thermal conductivity of the CNTs[9] grown in the thickness direction improves the transverse thermal conductivity of the base composite by about 50%. The electrical conductivity of the 3D composite was also measured and compared with that of the base composite (see the Methods section). The average through-thickness conductivity of the 3D composite (0.408 S cm^{-1}) was significantly higher than that of its 2D counterpart (0.075×10^{-6} S cm^{-1}). The measured average in-plane electrical conductivities of the 3D composite and base composite are 3.44 S cm^{-1} and 0.75×10^{-6} S cm^{-1}, respectively; indicating that the strong influence of the interfacial nanotubes provides conducting paths along all directions in the 3D composite structure. The much-improved through-thickness electrical conductivity observed in the 3D composites would potentially impart to these structures an electrical sensing capability for structural health monitoring during crack propagation or delamination.

The multifunctional 3D composite introduced here is the first real instance where the nanotubes are used in a value-added proposition to effectively improve traditional composite performance. The vertical arrays of nanotubes in the thickness direction of the composite improve the mechanical properties without compromising the in-plane properties, and also alleviate the problem of agglomeration when nanotubes are randomly introduced in the composites. Our results could pave the way for the application of CNTs in structural composite materials.

METHODS

DCB TEST PROCEDURE AND DATA REDUCTION

We used ASTM D5528-01 (test method for mode I interlaminar fracture toughness of unidirectional fibre-reinforced polymer matrix composites, ASTM, West Conshohocken, Pennsylvania, 2001). In this case, the two layered composite specimens were about 120-mm long and 20-mm wide. To avoid bending failure at the root of the specimen arms, sheet-metal tabs were bonded on each side of the specimen. A pre-crack was introduced in the mid-surface of the laminates by inserting a 12.5-μm Teflon film. The crack length, that is, the distance between the load application and the crack tip, was about 13 mm. The specimen edges were painted with a white brittle coating, and vertical lines were marked every 1 mm to record the crack length with loading. To load the specimens, hinges were adhesively attached to either side of the specimen. The specimens were loaded using an Instron 4206 testing machine. Corresponding to each 1-mm crack growth from the crack tip, the load (P) and displacements

(δ) were marked on the chart. The fracture toughness (G_{IC}) was reduced using equation (1) (ref. 17).

$$G_{IC} = \frac{nP_C\delta_C}{2wa}, \quad (1)$$

where n is the slope of $\log(\delta_C/P_C)$ versus $\log a$. P_C and δ_C are the critical load and the critical crack length.

ENF TEST DATA REDUCTION

The value of G_{IIC} was calculated using equation (2) (ref. 17).

$$G_{IIC} = \frac{9a^2P^2C}{4wL^3[1+1.5(a/L)^3]}, \quad (2)$$

where, a, P, C, w, and L represent initial crack length, load at the onset of nonlinearity, compliance of the linear region in the chart, width of the specimen, and half the span length in the three-point flexure, respectively. In equation (2), we did not consider the compliance correction factor from the interlaminar shear deformation, as in our case, G_{IIC} is only used for comparison purposes.

NANO-INDENTATION TEST PROCEDURE

We followed the procedure in the Product Data Sheet (MTS Nano Instruments, Oak Ridge, Tennessee, 2005). In the indentation test, a hard tip is pressed into the sample with a known load for a short time. Hardness for nanoindentation is defined as the ratio of maximum load to the residual indentation area. Before the test, the samples were polished using 0.5-μm grit until they were sufficiently smooth. A fast-curing epoxy was used to adhere the test sample to an aluminium stub. The loading increment was maintained as 5% of the present load per second. The samples were subjected to indentation at variable loads and indentation depths. Ten indentations were carried out at each depth and the average result was measured. Experiments were terminated at a depth of approximately 1 μm. The dynamic-contact module has 0.2-pm displacement resolution and 1-nN load resolution.

COEFFICIENT OF THERMAL EXPANSION MEASUREMENT PROCEDURE

We used ASTM E228-95 (standard test for linear thermal expansion of solid materials with a vitreous silica dilatometer). Three specimens with dimensions 5.1 mm × 5.1 mm × 7.6 mm with sanded-smooth surfaces were each placed between two 3.2-mm quartz cubes. The stacks were then spaced circumferentially around a 25.4-mm-diameter central hole in a 76.2-mm quartz plate. A 50.8-mm-diameter, 53-g quartz mirror was placed on top of the three cube/specimen stacks. A second thin mirror was placed on the surface of the 76.2-mm-diameter quartz plate located such that it was covering a part of the 25.4-mm hole in the 76.2-mm-diameter quartz plate. The interferometer was set up in a vertical mode with the beams reflecting off the upper and lower mirror surfaces. The quartz cubes were in the measurement path, and the resulting expansion of the cubes was subtracted from the measured data. Thermocouples were attached with Mylar tape to the quartz plate near where the specimens were located to monitor the specimen temperature. The chamber was evacuated to below 200 mtorr. Specimens were heated to 150 °C and held until they reached a stable thickness. Measurements were taken as the specimen temperature was cycled between the temperatures 150–0 °C for at least 1 full temperature cycle. Specimen thickness change and temperature were continuously recorded during the tests.

THERMAL CONDUCTIVITY MEASUREMENT PROCEDURE

We used ASTM E1530-99. A specimen (of size $A = 25.4$ mm × 25.4 mm) was placed under a uniform compressive load between two polished surfaces, which were kept at different controlled temperatures. The contact resistance was kept small by applying a reproducible pneumatic load to the test stack. The direction of heat flow was from the upper surface through the specimen to the lower surface. Once the thermal equilibrium was attained, the temperature difference (ΔT) across the specimen (ΔX) was measured along with the output from the heat-flow transducer (Q). The thermal conductivity, K, can be found from equation (3)

$$Q = -KA\frac{\Delta T}{\Delta X}. \quad (3)$$

ELECTRICAL CONDUCTIVITY MEASUREMENT PROCEDURE

The surfaces of the composite specimens were polished and metal (gold) contacts were deposited. We used a two-probe measuring method (see inset Supplementary Information, Fig. S4a), and the I–V plots (see Supplementary Information, Fig. S4) were used to calculate the conductivities of the two composites.

Received 12 January 2006; accepted 3 April 2006; published 7 May 2006.

References

1. Tong, L., Mouritz, A. P. & Bannister, M. *3D Fibre Reinforced Polymer Composites* (Elsevier Science, Oxford, 2002).
2. Dow, M. B. & Dexter, H. B. Development of stitched, braided and woven composite structures in the ACT program and at Langley Research Center. *NASA Technical Report* <http://techreports.larc.nasa.gov/ltrs/PDF/1997/tp/NASA-97-tp206234.pdf> 1–5 (1997).
3. Dresselhaus, M. S., Dresselhaus, G. & Eklund, P. C. *Science of Fullerenes and Carbon Nanotubes* (Academic, San Diego, 1996).
4. Baughman, R. H., Zakhidov, A. A. & de Heer, W. A. Carbon nanotubes-the route toward applications. *Science* **297,** 787–792 (2002).
5. Mouritz, A. P. Fracture and tensile fatigue properties of stitched fibreglass composites. *J. Mater. Des. Appl.* **218,** 87–93 (2004).
6. Dexter, H. B. & Funk, J. G. in *27th AIAA Structural Dynamics and Materials Conference (San Antonio, TX) AIAA Paper 86-1020* 700–709 (American Institute of Aeronautics and Astronautics, New York, 1986).
7. Tai, N. H., Yeh, M. K. & Liu, J. H. Enhancement of the mechanical properties of carbon nanotube/phenolic composites using a carbon nanotube network as the reinforcement. *Carbon* **42,** 774–777 (2004).
8. Thostenson, E. T., Li, C. & Chou, T. W. Nanocomposites in context. *Compos. Sci. Technol.* **65,** 491–516 (2005).
9. Ruoff, R. S. & Lorents, D. C. Mechanical and thermal properties of carbon nanotubes. *Carbon* **33,** 925–930 (1995).
10. Yu, M. F. *et al.* Strength and breaking mechanism of multiwalled carbon nanotubes under tensile load. *Science* **287,** 637–640 (2000).
11. Calvert, P. Nanotube composites: a recipe for strength. *Nature* **399,** 210–211 (1999).
12. Andrews, R. *et al.* Continuous production of aligned carbon nanotubes: a step closer to commercial realization. *Chem. Phys. Lett.* **303,** 467–474 (1999).
13. Mazumdar, S. K. *Composites Manufacturing: Materials, Product, and Process Engineering* (CRC Press, Boca Raton, 2002).
14. Cao, A. *et al.* Multifunctional brushes made from carbon nanotubes. *Nature Mater.* **4,** 540–545 (2005).
15. Ghasemi-Nejhad, M. N., Chandramouli, M. V. & Yousefpour, A. Processing and performance of continuous fiber ceramic composites by preceramic polymer pyrolysis: I—filament winding. *J. Compos. Mater.* **35,** 2207–2237 (2001).
16. Ghasemi-Nejhad, M. N., Bayliss, J. K. & Yousefpour, A. Processing and performance of continuous fiber ceramic composites by preceramic polymer pyrolysis: II—resin transfer molding. *J. Compos. Mater.* **35,** 2239–2255 (2001).
17. Adams, D. F., Carlsson, L. A. & Pipes, R. B. *Experimental Characterization of Advanced Composite Materials* 3rd edn (CRC Press, Boca Raton, 2003).
18. Martin, R. H. in *Proc. Am. Soc. Compos. Third Technical Conference (Seattle, Washington)* 688–701 (Technomic, Lancaster, Pennsylvania, 1988).
19. Prel, Y. J., Davies, P., Benzeggagh, M. L. & de Charentenay, F. *Composite Materials: Fatigue and Fracture, Proc. 2nd. Symp. (Cincinnati, Ohio)* Vol. 2 , 251–269 (American Society for Testing and Materials, Philadelphia, Pennsylvania, 1989).
20. Koratkar, N., Wei, B. & Ajayan, P. M. Carbon nanotube films for damping applications. *Adv. Mater.* **14,** 997–1000 (2002).
21. Zhang, M., Atkinson, K. R. & Baughman, R. H. Multifunctional carbon nanotube yarns by downsizing an ancient technology. *Science* **306,** 1358–1361 (2004).
22. Zhou, X., Shin, E., Wang, K. W. & Bakis, C. E. Interfacial damping characteristics of carbon nanotube-based composites. *Compos. Sci. Technol.* **64,** 2425–2437 (2004).
23. Kwon, Y-K., Berber, S. & Tománek, D. Thermal contraction of carbon fullerenes and nanotubes. *Phys. Rev. Lett.* **92,** 015901 (2004).

Acknowledgements

We thank B. Crawford of MTS Nano Instruments, for many helpful discussions. V.P.V. and M.N.G.-N. acknowledge the support of the ADPICAS project funded by the Office of Naval Research under government grant numbers N00014-00-1-0692 and N00014-05-1-0586. A.C. acknowledges the ADPICAS project as well as the start-up support from the College of Engineering and the Department of Mechanical Engineering at the University of Hawaii at Manoa. P.M.A. acknowledges the support of the Focus Center of New York for Electronic Interconnects and the NSF Nanoscale Science and Engineering Center for the directed assembly of nanostructures.
Correspondence and requests for materials should be addressed to V.P.V. or M.N.G.-N.
Supplementary Information accompanies this paper on www.nature.com/naturematerials.

Competing financial interests

The authors declare that they have no competing financial interests.